2001

Mon. Not. R. Astron. Soc. **000**, 000–000 (2002)

The systemic velocities of four long-period cataclysmic variable stars

R. C. North[1,4], T. R. Marsh[1⋆], U. Kolb[2], V. S. Dhillon[3] and C. K. J. Moran[1]
[1] *University of Southampton, Department of Physics & Astronomy, Highfield, Southampton SO17 1BJ*
[2] *The Open University, Department of Physics & Astronomy, Walton Hall, Milton Keynes, MK7 6AA*
[3] *University of Sheffield, Department of Physics & Astronomy, Sheffield, S3 7RH*
[4] *Met Office, London Road, Bracknell, Berkshire, RG12 2SZ*

Accepted Received in original form

ABSTRACT

Although a large number of orbital periods of cataclysmic variable stars (CVs) have been measured, comparison of period and luminosity distributions with evolutionary theory is affected by strong selection effects. A test has been discovered which is independent of these selection effects and is based upon the kinematics of CVs (Kolb & Stehle, 1996). If the standard models of evolution are correct then long-period ($P_{\rm orb} > 5$hrs) CVs should be typically less than 1.5 Gyr old, and their line-of-sight velocity dispersion (σ_γ) should be small. We present results from a pilot study which indicate that this postulate is indeed true. Four long-period dwarf novae (EM Cyg, V426 Oph, SS Cyg and AH Her) were observed over a complete orbit, in order that accurate radial velocities be obtained. We find values of -1.7, 5.4, 15.4 and 1.8 $\mathrm{km\,s^{-1}}$ with uncertainties of order 3 $\mathrm{km\,s^{-1}}$, referred to the dynamical Local Standard of Rest (LSR), leading to a dispersion of $\sim$8 $\mathrm{km\,s^{-1}}$. Calculation of a 95 per cent confidence interval gives the result $4 < \sigma_\gamma < 28\,\mathrm{km\,s^{-1}}$ compared to a prediction of 15 $\mathrm{km\,s^{-1}}$. We also have an improved determination of mass donor spectral type, K_2 and q for the four systems.

Key words: binaries: spectroscopic – novae, cataclysmic variables – accretion, accretion discs – techniques: radial velocities

1 INTRODUCTION

Dwarf novae (DN) are a sub-group of cataclysmic variable stars. They consist of a white dwarf (primary) star accreting matter from a red dwarf (hereafter 'mass donor') which is in contact with its Roche lobe. The material streams from the mass donor through the inner Lagrangian point into the potential well of the primary, where it impacts onto the outer edge of an accretion disc. Observable features which distinguish DN from other CVs are the outbursts which occur on a regular basis (with a baseline from days to months) and cause the system to increase in brightness by $m_v \approx 2-5$ magnitudes.

The mass transfer process in CVs is driven by orbital angular momentum loss. Gravitational radiation is highly effective at short orbital periods, and theoretical calculations reproduce well the observed mass transfer rates in CVs. For longer period systems, with higher mass transfer rates, an alternative mechanism is needed. This is widely accepted to be *magnetic braking*, a spin-down effect on the mass donor due to a stellar wind that effectively co-rotates with its magnetic field. Due to effective tidal locking in CVs, the mass donor will not slow down, and instead angular momentum is extracted from the binary orbit. However, magnetic braking still remains only a hypothesis, and the level of direct observational support is still low.

In the standard model for the formation and evolution of CVs magnetic braking is only active for donor stars with a radiative core. Hence there is a marked difference between the evolutionary time scale of systems above the period gap ($P_{\rm orb}3\,$h) and those below the gap ($P_{\rm orb}2\,$h). Kolb & Stehle (1996) used population synthesis methods to confirm this. They determined the age structure of a model population of Galactic CVs, and by convolving this with the observed age-space velocity relation of Wielen et al. (1992) (which is believed to result from the diffusion of stellar orbits due to gravitational interactions with massive objects) obtained the theoretical distribution of systemic, hereafter γ, velocities. They showed that the age of a system in the present CV population is largely determined by the timescales of the orbital angular-momentum loss mechanisms. In addition, the models showed that the brightness-dependent

⋆ email: trm@astro.soton.ac.uk

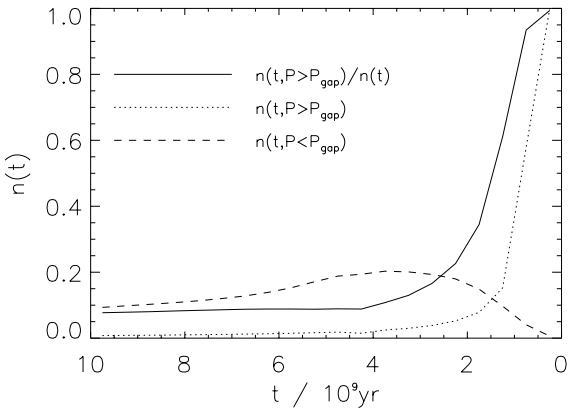

Figure 1. The figure (from Kolb & Stehle, 1996) shows the relative number of systems as a function of age, for CVs above the period gap ($P_{\rm orb} > 3$hr, dotted line) and below the gap ($P_{\rm orb} < 2$ hr, dashed line). The solid line is the total fraction of CVs above the period gap as a function of age. The relative youth of the longer period systems is a firm prediction of the magnetic braking model of CV evolution.

selection effects which have hitherto plagued comparisons between observations and theory preserve the age differences, thereby providing an opportunity to test directly the magnetic braking model. So, if the standard models are correct, then the CVs having periods longer than the upper limit of the period gap ($P_{\rm orb} \geq 3$ hours) should be younger (≤ 1.5Gyr), and therefore have a smaller line-of-sight velocity dispersion according to the empirical age–velocity dispersion relation (predicted value ~ 15 km s^{-1}).

Conversely, those CVs with orbital periods shorter than the lower limit of the period gap, should be older ($\geq$ 3-4Gyr) and show a larger velocity dispersion (predicted as ~ 30 km s^{-1}).

In a review by van Paradijs, Augusteijn & Stehle (1996), the observed γ velocities for a sample of CVs were collected from published radial-velocity studies and statistically analysed. They could detect no difference between the velocity dispersions for below-gap and above-gap objects (see section 5). All their data were taken from the literature, and they assumed that there was no significant difference between measurements taken from emission and absorption line measurements in their sample. The problems associated with using values taken from the literature are not negligible. The γ velocity is a measure of the centre-of-mass radial velocity of the binary star, and can be deduced directly from radial velocity curves. Typically with the emission lines from CVs, a γ-value which is only one tenth the size of the radial velocity variations in the system, and only one hundredth of the total spectral line width, is being measured. The radial velocities obtained from emission lines are well known to be affected by the internal motions in the disc or stream. Therefore, the measurements of γ obtained from emission lines may not accurately reflect the motion of the white dwarf at all. This will be especially true if the inner disc is distorted in some way, for example, in magnetic CVs where the field on the primary is so strong it disrupts the accretion disc and disrupts the accretion disc near to the surface of the white dwarf. Measuring radial velocities from the absorption lines due to the mass donor helps reduce potential sources of error. However, these absorption lines are not visible in all dwarf novae. They are generally only present in those systems with orbital periods above the period gap.

Many radial-velocity curves for different CV systems have been constructed. However, if the only requirement is a measurement of the radial velocity semi-amplitude, care will not have been taken to ensure that systematic errors do not dominate. It is vital that spectra are adequately sampled, and that a reasonable number of radial velocity standards have been observed. If a lower resolution is used to obtain data, then the probability of the spectral lines being affected by blending is significantly increased.

Here, we present the initial results of a project to deduce reliable γ velocities for a large sample of longer-period ($P_{\rm orb} \geq 6$ hours) non-magnetic CVs. The aim of this initial investigation was to test the methods and procedures described in §III, to see whether they could produce sufficiently accurate absolute γ velocity values, capable of being used to construct an observed velocity-dispersion relation for Galactic CVs, and thus for comparing directly with the theory.

2 OBSERVATIONS

During five nights starting from 19th June 1997, high time-resolution spectroscopy was carried out using the Intermediate Dispersion Spectrograph (IDS), on the 2.5-m Isaac Newton Telescope (INT) on the island of La Palma, on four longer period ($P_{\rm orb} > 6$ hours) DN. The objects observed are listed with exposure times and orbital periods in Table 1. Conditions were clear throughout the five nights of observing, and the seeing was approximately 1 arc sec. Spectra of radial-velocity standard stars were also obtained to calibrate the velocities measured from the DN. They were also used to obtain a spectral type for the mass donor in each DN, and so only those with good spectral types were chosen. These were selected from the lists of Marcy, Lindsay & Wilson (1987), Barnes, Moffett & Slovak (1986), Beavers et al. (1979), Duquennoy, Mayor & Halbwachs (1991) and Eggen (1996). The spectra covered the wavelength range from $6220 - 6640$Å, which includes absorption lines from the mass donor around $6350 - 6500$Å and the Hα emission line at 6563Å. All the spectra had a dispersion of 0.4 Å per pixel, resulting in a resolution with the 500-camera of 0.8Å (FWHM). Each DN exposure was of the order of $\simeq 200$ – 300 seconds, in order to keep sufficient phase resolution that no orbital smearing would be introduced. The DN observed all had orbital periods in the range $025 \leq P_{\rm orb} \leq 029$, and were tracked for a minimum of 6 hours at one time. The 0.8 arc sec wide slit was rotated in order to capture the spectrum of both the DN and a second star on the slit, to correct for slit losses.

The CCD frames were bias-subtracted and flat-fielded. Variations in the illumination of the slit were corrected using exposures of the twilight sky. The object spectra were extracted using the optimal weighting technique of

Table 1. A summary of the observations taken in June 1997 on the 2.5-m INT. All used the IDS 500-mm camera with the Tek CCD chip and R1200Y grating giving a dispersion of 0.4Å per pixel, and resulting in a resolution of 0.8Å (FWHM).

Object	Date observed (UT, June 1997)	T_{exp} (s)	$P_{\rm orb}$ (days)	Reference
EM Cyg	21.93-22.22	200	0.290909	[1]
V426 Oph	20.92-21.21	200	0.285314	[2]
SS Cyg	23.01-23.23	200	0.27512973	[3]
AH Her	19.91-20.17	300	0.258116	[4]

References: (1) Stover et al., 1981 ; (2) Hessman, 1988; (3) Hessman et al., 1984; (4) Horne, Wade & Szkody, 1986.

Horne (1986). Arc calibration spectra were taken approximately every half hour, and with each change of object. They were fitted with fourth-order polynomials, which had an rms scatter of 0.005Å. The spectra were corrected onto a flux scale using a flux standard from Oke & Gunn (1983).

3 METHODS

The γ velocities needed to be measured to within 5 $\rm km\,s^{-1}$ so that a velocity dispersion of the order 15 $\rm km\,s^{-1}$ could be detected. The following process illustrates how this was achieved, and how potential sources of systematic error were minimised.

(i) First, the individual spectra of each DN were re-binned onto a logarithmic wavelength scale (Stover et al., 1980). Then each individual DN spectrum was cross-correlated with that of a radial-velocity standard (re-binned onto an identical scale), following the method of Tonry & Davis (1979), in order to determine heliocentric radial velocities. Adjustments were made at this stage to allow for the radial-velocity of the standard star. No allowance (at this stage) was made for the rotational broadening of the absorption lines from the mass donor.

(ii) The radial velocities were then fitted with a circular orbit fit of the form

$$V = \gamma + K \sin \frac{2\pi(t - t_0)}{P_{\rm orb}} \qquad (1)$$

to calculate the radial-velocity semi-amplitude (K), the systemic velocity (γ), and the phase-zero point where phase zero, ϕ_0, is defined as the phase at which the radial velocity of the mass donor crosses zero moving from negative to positive (see Section 4.1). These initial radial velocity fits were made to allow the orbital motion of the mass donor to be removed from the individual spectra in order to create an average spectrum from which to determine the spectral type.

(iii) Repeated (ii) using radial-velocity standards artificially broadened to match the widths of the absorption lines seen in the DN. Measurements of the rotational broadening of the absorption lines are discussed in section 4.2.

(iv) An estimate of the mass donor spectral type could be deduced simply by inspection of the spectra (see North et al., 2000, and section 4.3) An alternative method used is discussed in section 4.3 together with the results obtained.

(v) Finally, the cross-correlation was repeated again, using the radial-velocity standard (of best-fitting spectral-type) broadened to the measured rotational velocity of the mass donor.

To avoid introducing errors due to spectral-type mismatch between standard star and DN, steps (i) to (v) were repeated with velocity standards of several different spectral types (ranging from G8V–M6V). The radial velocities obtained for each DN did not differ significantly, implying that this is not a large source of systematic error here.

4 RESULTS

In this section, the results obtained using the methods described in section 3 are presented. Section 4.1 describes the radial velocities obtained for each mass donor. This is followed by the results of the rotational broadening measurements (section 4.2), and the mass-donor spectral typing process (section 4.3). The resulting γ velocities are given in section 4.4. Finally Doppler maps of the Hα emission are presented in section 4.6.

4.1 Mass donor radial velocity curves

To obtain radial velocities, the absorption spectrum from the mass donor, which can be seen in the wavelength region $\lambda\lambda\,6350 - 6540$ Å was used. The absorption lines from the mass donor are easily distinguished from interstellar features, as they exhibit a sinusoidal variation. The trailed spectra in Fig. 2 show the behaviour of the spectral lines over a full orbital period as observed in each system. Figure 2 clearly shows the sinusoidal behaviour of the absorption lines. Each panel also shows how the emission lines vary approximately 180 out of phase with the absorption lines. The lines at ≈ 6300 Å are interstellar absorption. The difference between the trails of the individual systems are apparent in this plot. For example, the absorption lines in AH Her are barely visible, whereas those in SS Cyg are very obvious. All the objects were observed when the system was in or approaching a quiescent disc state. Also, the strength of the absorption lines may vary around the binary orbit if the hemisphere of the mass-donor facing the white dwarf is being irradiated by the accretion disc and boundary layer. This manifests itself as a departure from a circular orbit fit to the radial velocities around phase 0.5 (see Fig. 3). The behaviour of the Hα line is also seen to differ markedly in each object. This is discussed in section 4.6.

The radial velocities resulting from the cross-correlation procedure were fit with a sine curve, to determine the semi-amplitude, K_2, phase-zero point, ϕ_0, and γ velocity. The orbital periods are already well-determined for the four observed DN, so we use the values given in the literature (see Table 1 for details). Figure 3 shows the sinusoidal fits to the radial velocities of each DN. The radial-velocity standard used to obtain each fit was of best-fitting spectral type and artificially broadened to the value obtained in section 4.2.

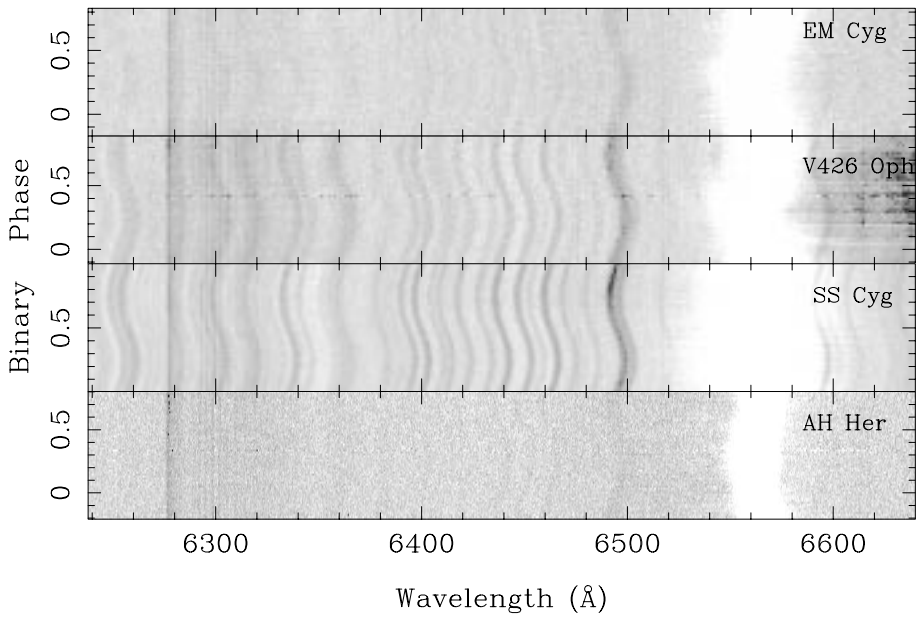

Figure 2. Trailed spectra (wavelength versus binary phase) of the DN observed, scaled to ±0.2 of the continuum level. The Hα lines have been saturated (white) in order to bring up the contrast of the absorption lines from the mass donor, which can be seen in the wavelength range 6300–6500 Å. From top-to-bottom, the panels show the systems in descending orbital period length. In V426 Oph and SS Cyg, the sinusoidal nature of the absorption lines (black) is clearly visible. The lowest panel contains the trailed spectra of AH Her. The mass donor lines are not as clear as in all the other dwarf novae, but the feature at λ 6495 Å is visible. The absorption lines in EM Cyg have been corrected for the presence of an additional late-type spectrum (see North et al., 2000). See Fig. 7 for Hα detail.

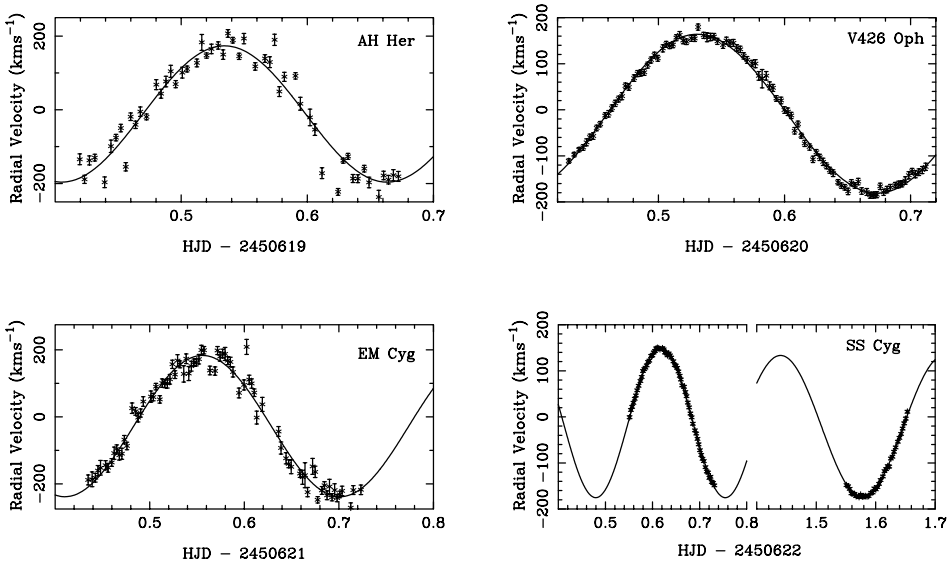

Figure 3. Sinusoidal fits to the radial velocity data for each dwarf nova. Clockwise from top left, AH Her, V426 Oph, EM Cyg and SS Cyg. The data from two nights worth of observations for SS Cyg is combined into the lower right-hand plot.

Table 2. Orbital parameters determined from the absorption line radial velocity curves

Object	K_2 ($\mathrm{km\,s^{-1}}$)	ϕ_0[a] 2450000+
EM Cyg	202±3	621.4833(5)
V426 Oph	179±2	620.4596(3)
SS Cyg	165±1	622.5483(2)
AH Her	175±2	619.4669(5)

[a] Figure in brackets is the error on the final digit.

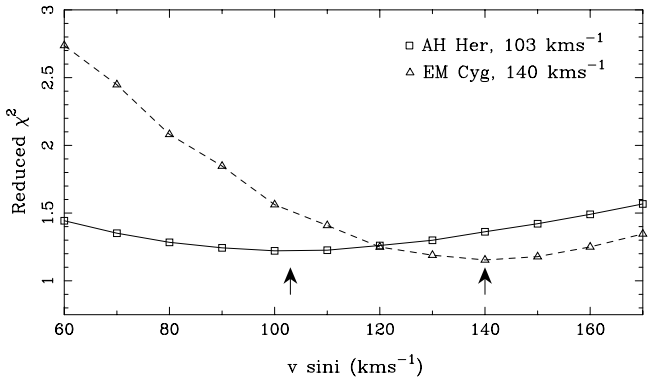

Figure 4. Examples of the χ^2 versus $v \sin i$ curves obtained during the rotational broadening measurement procedure. The arrows denote the positions of the minima of the curves (optimum $v \sin i$ value).

4.2 Projected rotational velocities of the mass donors

The rotational broadening of the absorption lines was determined by artificially broadening the radial velocity standards to values between 0 and 200 $\mathrm{km\,s^{-1}}$ (using increments of $10\,\mathrm{km\,s^{-1}}$). The orbital motion of the mass donor was removed from the individual CV spectra, and the results rebinned onto a uniform velocity scale. The resulting spectra were then co-added. The fraction of each broadened standard which best removed the mass-donor lines was then calculated, using an optimisation technique which minimised the scatter between the spectrum of the standard and the DN spectrum. Plotting χ^2 versus the amount of artificial broadening used on the standard produces a minimum in χ^2 at the optimum value of $v \sin i$ (see Fig. 4 for examples). This gave a value for the rotational broadening of the mass donor. In order to check that choosing one spectral type for the mass donor did not introduce a further source of systematic error, we repeated the $v \sin i$ measuring technique with all the available standard stars. The standard error on the mean of the sample was $2\,\mathrm{km\,s^{-1}}$, implying that the choice of standard used to calculate $v \sin i$ was not significant. A value of 0.5 was used for the limb-darkening coefficient for each DN. Changing this value over the range $0-1$ did not alter the deduced values of $v \sin i$ by more than $5\,\mathrm{km\,s^{-1}}$, see North et al. (2000) for details of the method followed. Table 3 shows the measurements of $v \sin i$ for each of the observed systems. Horne, Wade & Szkody (1986) calculated a value for the rotational broadening of the mass donor in AH Her of 112±17 $\mathrm{km\,s^{-1}}$. Our value of 103±2 $\mathrm{km\,s^{-1}}$ agrees with theirs. Hessman (1988) determines a value for the mass donor of SS Cyg of 87±4 $\mathrm{km\,s^{-1}}$. Our value of 96±3 $\mathrm{km\,s^{-1}}$ agrees at the 2σ level.

Table 3. Results of the procedure to find the value of the rotational broadening of the mass donor in the four DN.

Object	$v \sin i$ ($\mathrm{km\,s^{-1}}$)	Spectral type of standard used	mass ratio from $v \sin i$ and K_2
EM Cyg	140 ± 2	K3V	0.88 ± 0.03
V426 Oph	132 ± 3	K5V	0.96 ± 0.01
SS Cyg	96 ± 3	K5V	0.68 ± 0.02
AH Her	103 ± 2	K7V	0.69 ± 0.02

4.3 Mass donor spectral types

The radial-velocity standard spectra were each artificially broadened to an appropriate value (that determined in section 4.2). Then the fraction of that broadened standard which, when subtracted from the DN spectrum best removed the spectral lines of the mass donor was calculated. The routine used minimised χ^2 between the DN spectrum (with a specific fraction of the chosen standard subtracted) and a smoothed version of itself. The standard producing the lowest value of χ^2 gave an indication of the mass donor spectral type. All the objects observed have mass donors with a spectral type later than K3. AH Her best fitted a K7V mass donor. SS Cyg and V426 Oph were both best-fit using a K5V spectral type. Finally, EM Cyg resulted in a $\mathrm{K3}-5$ type mass donor (see North et al. (2000)).

Figure 5a shows the average spectra of the four DN, created by removing the orbital motion of the mass donor from each individual spectrum, re-binning onto a uniform velocity scale and co-adding the results. The absorption lines are obviously broadened (c.f. those of Figure 5b); measured in each case to be $\approx 100\,\mathrm{km\,s^{-1}}$, see Table 3. Marked on the plot are a few of the spectral lines found most useful in the spectral typing process. The blend at λ6495 is also marked on the plot. It is a blend of mostly Ca I λ6493.8 and Fe I $\lambda\lambda$6495.0, 6495.7 and λ6496.5. However, it is the one absorption feature originating from the mass donor which is clearly visible in the trailed spectra of each object. Purely by inspection, there appear to be four reliable indicators of spectral type in this wavelength range (see Fig. 5a). First, there appears to be a relationship between the relative depths of λ6439.1 and the blend at $\approx$ λ6400 which changes rapidly over the spectral type range we are interested in here. Secondly, the Fe I lines around λ6400 begin to change very obviously around spectral type K7. The general shape of the spectrum around 6370Å allows us to deduce whether the mass donor is a K- or M-type star. Finally, the two spectral features just short of the λ6495 blend vary significantly relative to each other over the spectral range G8–M6. Figure 5b shows a range of typical standard star spectra covering spectral types G8V to M5V for comparison.

Table 4. The mass donor spectral type determined for each object. Previous estimates of the spectral type (from the literature) are also given.

Object	Spectral Type of mass donor	Previous Spectral type	Fraction contribution of mass donor	reference for previous type[a]
EM Cyg	K3	K5V	0.231±0.005	3
V426 Oph	K5V	K3V	0.336±0.006	2
SS Cyg	K5V	K2-K3V	0.685±0.004	4
AH Her	K7V	K0-K5V	0.102±0.006	1

[a] 1) Horne, Wade & Szkody, 1986; 2) Hessman, 1988; 3) Stover et al., 1981; 4) Martinez-Pais et al., 1994.

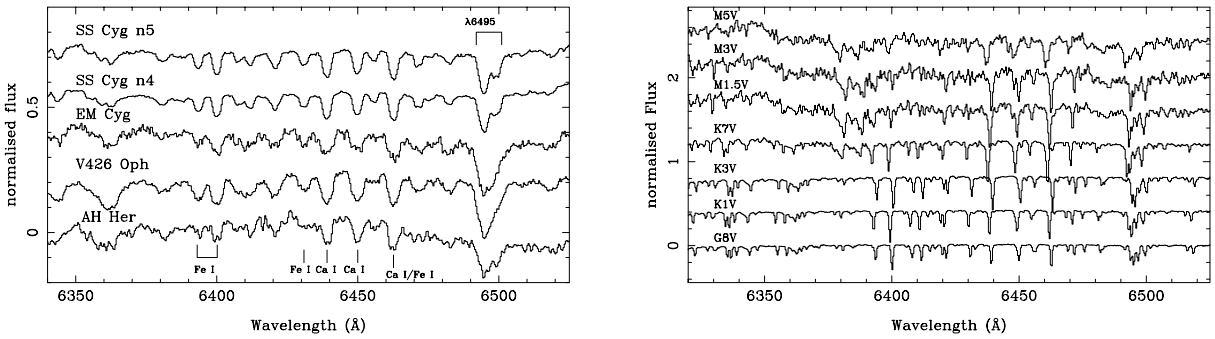

Figure 5. Left. a) The average spectra of the mass donors of the four DN observed. The raw spectra for each DN have had the orbital motion of the mass donor removed, then been re-binned onto a uniform velocity scale and averaged. **Right** b) A selection of the radial velocity standards observed, ranging from the earliest spectral type observed (G8V) to the latest (M5V)

Table 5. Heliocentric γ velocities for four dwarf novae, and corrections for the solar motion

Object	Heliocentric γ velocity ($\mathrm{km\,s^{-1}}$)	Correction for solar motion ($\mathrm{km\,s^{-1}}$)	Absolute γ velocity ($\mathrm{km\,s^{-1}}$)
EM Cyg	-27.38±1.88	-25.65	-1.74±1.9
V426 Oph	-11.07±0.84	-16.46	5.4±0.8
SS Cyg	-13.09±2.88	-28.52	15.4±3.0
AH Her	-5.99±1.54	-7.75	1.8±1.5

4.4 Deducing the γ velocities

There have been many radial-velocity studies on DN which have published γ velocity values, both for DN in outburst and quiescence. Several of these results do not appear consistent with each other. We believe that this is just a symptom of the data acquisition methods. Obtaining γ velocities is not the primary aim for many of these studies, and so it is highly probable that the spectra are undersampled and therefore unsuitable for deducing absolute γ velocity values.

The γ velocities are calculated at the point in the analysis described previously when the final radial-velocity curves are derived for each object. They are deduced using a sinusoidal fit to the radial velocities around the complete orbit, which have themselves been determined using a standard of the same spectral type as the mass donor, which has been artificially broadened to the measured $v \sin i$. The values calculated at this point are heliocentric, and in order to deduce the velocity dispersion for these measurements, it was necessary to correct for the solar motion. For this we used the dynamical Local Standard of Rest (LSR) as the reference point (Wallace & Clayton, 1999). Figure 6 shows the range of γ values obtained for each spectral type of radial-velocity standard, for each DN. It was here that using so many radial-velocity standard stars was most useful. Table 5 shows the best-fitting heliocentric γ velocity values for each object, and the velocity shift applied (in $\mathrm{km\,s^{-1}}$) to correct for the solar motion. Most of the derived γ velocity values for each dwarf nova are consistent to within the error margin of $\pm 2\,\mathrm{km\,s^{-1}}$.

Considering only the data obtained here, the velocity dispersion, σ_γ, appears to be approximately $8\,\mathrm{km\,s^{-1}}$, smaller than the value of $15\,\mathrm{km\,s^{-1}}$ predicted by Kolb & Stehle for longer period systems, yet still consistent with it. We calculate a 95 per cent confidence limit on the value of σ_γ to be $4 < \sigma_\gamma < 28\ \mathrm{km\,s^{-1}}$, a large range with only 4 systems. If the dispersion we measure is assumed to remain at the same magnitude but the number of measured systems increases to 8 then the 95 per cent confidence limit decreases to $5 < \sigma_\gamma < 16\ \mathrm{km\,s^{-1}}$.

In addition system parameters for the four DN were calculated using the derived values of $v \sin i$ and K_2 (see Table 6).

4.5 A note on the space velocity of SS Cyg

One of the observed DN (SS Cygni) has had its parallax measured using the Fine Guidance Sensor (FGS) on the Hubble Space Telescope (HST) (Harrison et al., 2000). The

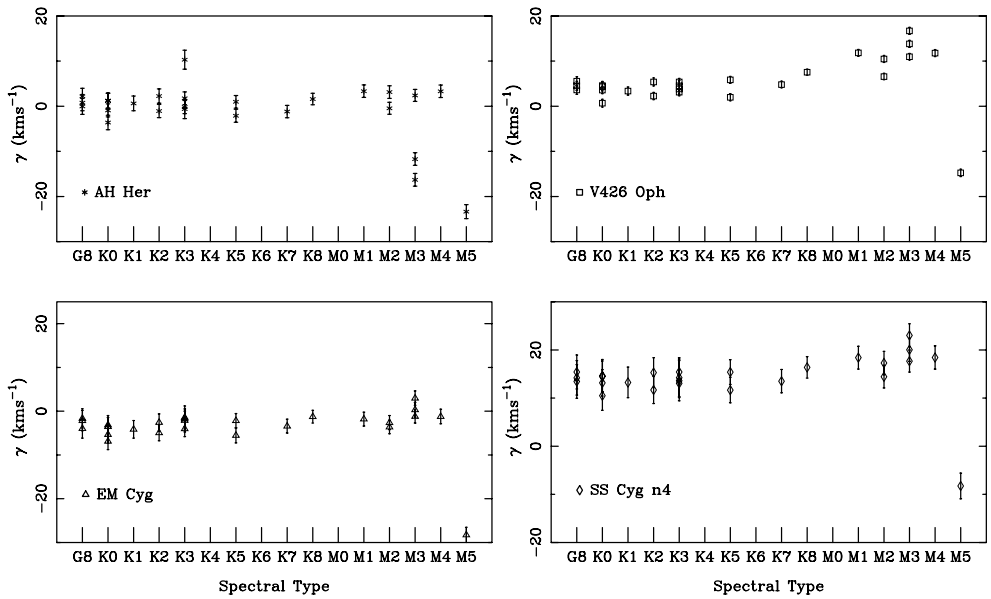

Figure 6. The γ velocities calculated with each spectral type standard.

Table 6. System parameters determined using the derived values of $v \sin i$ and K_2

Object	$M_2 \sin^3 i$ ($M_\odot$)	$M_1 \sin^3 i$ ($M_\odot$)	Inclination ()
EM Cyg	0.77±0.08	0.88±0.05	67±2[1]
V426 Oph	0.62±0.02	0.65±0.02	59±6[2]
SS Cyg	0.25±0.01	0.36±0.01	37±5[2]
AH Her	0.28±0.01	0.41±0.01	46±3[2]

[1] North et al. (2000), [2] Ritter & Kolb (1998)

parallax measurement of 6.02 ± 0.46 mas lead to a new distance for SS Cyg of 166 ± 12 pc, almost twice the distance obtained previously. The tangential velocity calculated using this distance is 93 km s^{-1}. So, although our radial velocity agrees with theoretical expectations, the total space velocity of 94 km s^{-1} does not.

It is possible that there is a problem with the SS Cyg parallax – for example Schreiber & Gäensicke have shown that the small parallax, and consequent implied luminosity causes problems with the disc instability theory. It causes us problems here too, although even if the distance were only 100 *pc* the space velocity would still be a relatively high 56 km s^{-1}. As SS Cyg is only one system, little can be deduced; it is clearly of interest for more parallaxes and proper motions to be measured.

4.6 Doppler Tomography

A useful method of imaging the accretion discs in CVs is Doppler tomography (Marsh & Horne, 1988). This procedure maps emission from the CV in velocity space, using a coordinate system which co-rotates with the binary star. Due to the synchronous rotation of the mass donor with the binary motion, the shape of the Roche lobe is conserved in velocity space, and can be plotted on the Doppler map. The aim of the observations, to measure accurate absolute γ velocities, means that these data are ideal for applying Doppler tomography methods, in this case to the Hα emission line. Figure 7 is a compilation of the Doppler maps of the Hα emission for the four systems. The uppermost panel shows the observed trailed spectra centred at 6562.760Å, using a velocity scale on the x-axis with a range of ± 900 km s^{-1}. The middle panel in each column plots the Doppler image. Finally, the lower panel presents the computed trailed spectra, as reconstructed from the Doppler images. The observed data are generally reproduced well, however several asymmetric features exist in the observed data which the software tried to fit and failed.

Starting with the plots for AH Her (column four of Fig. 7), it can be seen in the trailed spectra that there are two obvious 'S-wave' components. One of these is from the mass donor (starting at -100 km s^{-1} at phase -0.2). It manifests itself in the Doppler map at velocities indicating an origin on the irradiated hemisphere (that facing the white-dwarf and boundary layer) of the mass donor. The second 'S-wave' feature is travelling in phase with the general trend of the Hα line, thus following the motion of the accretion disc and white dwarf. It appears in the Doppler map as a smeared blob in the lower-central region. SS Cyg has a similar Doppler map (column three of Fig. 7). There is a prominent contribution from the hemisphere of the mass donor facing the white dwarf. In addition, there is a smeared blob here too, appearing this time in the bottom-to-lower-right quadrant of the Doppler map. The trailed spectra show a second 'S-wave' component moving in phase with the emission line, which apparently shifts from negative to positive velocity around phase 0.4/0.5. Both of the Doppler maps (for AH Her and SS Cyg) show emission at lower velocities than the predicted outer disc velocities for an accretion disc with a radius $0.8R_{L_1}$ (plotted as dot-dashed circles on the Doppler images), so-called "sub-Keplerian" velocities.

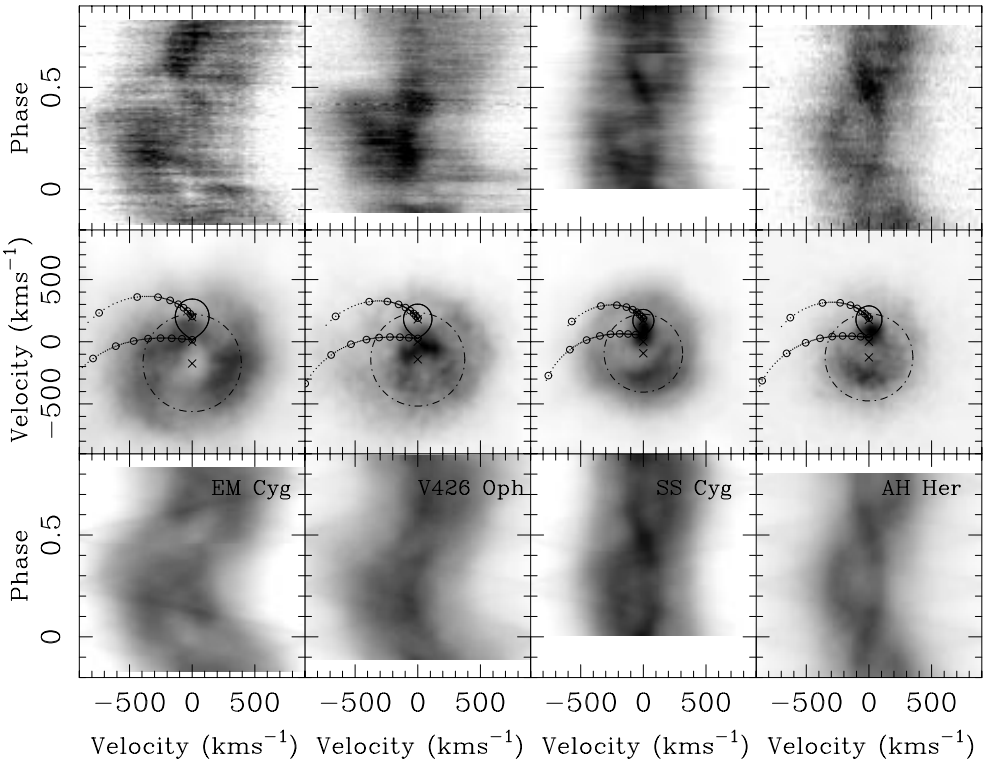

Figure 7. Doppler maps of the four dwarf novae. From left to right: EM Cyg, V426 Oph, SS Cyg and AH Her. From top to bottom, the panels show a) the actual data (in the form of trailed spectra); b) The Doppler map of the Hα emission; c) The data reconstructed from the Doppler map. The Roche lobes were plotted onto each Doppler map using the mass ratios given in Table 3 and the values of K_2 calculated in section 4.1. The predicted path of the gas stream is also shown, and open circles are marked on at $0.1\,R_{L_1}$ intervals. The upper path is the Keplerian velocity along the stream; the lower path is the direct velocity along it

V426 Oph has a very peculiar Hα map (see column two of Fig. 7). The emission appearing near zero velocity doesn't all fit into the Roche lobe of the mass donor. It appears to be consistent with the velocity of the inner Lagrangian point, but 'spread out' in a semi-circular fashion. The trail reconstructed from the Doppler map appears to have more structure than can be clearly seen in the actual data, however the feature seen in the actual data at phase 0.4 isn't reproduced in the predicted data. There is also an approximately steady emission varying at low velocities near the line centre. This produces the semi-circular emission feature in the Doppler image. The observed data also appear to show an eclipse at phase 0. This has not been observed in V426 Oph before. Not easily seen on the Doppler map is a region of emission at high velocities on the left-hand side. This may be an indication of stream overflow (Hellier, 2000). The emission line behaviour is reminiscent of the emission-line behaviour in the class of Nova-like variables, sometimes called the SW Sex stars (Thorstensen et al., 1991).

EM Cyg (in column one) again shows emission on the irradiated hemisphere of the mass donor (see North et al. (2000) for further discussion), and has the most ring-like feature indicative of an accretion disc. However, the peak velocities measured from this are again apparently sub-Keplerian.

5 DISCUSSION

Kolb & Stehle (1996) explain that the velocity dispersion (σ) is defined as the rms of the peculiar stellar space velocity, v in a local Galactic coordinate system (U,V,W), where U points towards the Galactic centre, V is in the direction of the Galactic rotation, and W is in the direction of the North Galactic pole. Wielen et al. (1992) (introduced by Wielen (1977)) deduced that the total dispersion, $\sigma_{\rm v}$ is defined by

$$\sigma_{\rm v}^2 = \sigma_V^2 + \sigma_U^2 + \sigma_W^2 \tag{2}$$

and obeys this empirical age–velocity relation:

$$\sigma_{\rm v} \simeq 10 + 21.5\left(\frac{t}{10^9{\rm yr}}\right)^{1/2}\ {\rm km\,s^{-1}}. \tag{3}$$

According to more recent studies there is some uncertainty surrounding this relation. For a short discussion on this point see Kolb (2001). In any case, this relation is also expected to hold for binary systems, unless an event occurs during the evolution in which a significant fraction of the total mass of the system is violently, asymmetrically ejected. In the case of CVs, the progenitors do eject a significant fraction of their mass during the common-envelope period, but this occurs on a time scale much longer than the duration of the orbital period, and so can be considered to be symmetric about the rotation axis of the binary. This means that the space velocity of the system is not affected. Kolb & Stehle note that repeated nova eruptions might alter the

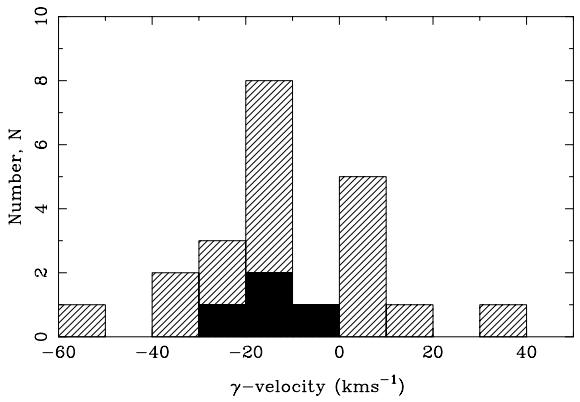

Figure 8. A histogram showing the spread of values for the γ velocities of the DN observed. The solid histogram shows the results we have so far, and the area with hatched lines denotes values for each of the observed systems gathered from the literature.

space velocity of the system. This would in effect *increase* the velocity dispersion of CVs. In this case, equation 3 would underestimate the total dispersion.

The characteristic velocity observed for the CV population is the velocity of the centre of mass of the binary system. Assuming CVs are isotropically distributed about the Galaxy, the observed γ velocity dispersion is related to $\sigma_{\rm v}$ by

$$\sigma^2_{|{\rm v}|} = <\gamma^2> = \frac{1}{3}\sigma^2_{\rm v} \qquad (4)$$

It is seen that the CVs above the period gap (young) show a significantly smaller dispersion in γ. What is notable about the $\sigma_\gamma(P_{\rm orb})$ distribution is that it is essentially *independent* of the selection effects which plague the original distribution, $n(P_{\rm orb})$. The observations described here are a first step towards a statistically meaningful sample of γ velocity measurements, for objects both above and, eventually, below the period gap in the distribution of CVs.

From the study of van Paradijs, Augusteijn & Stehle (1996), the 47 systems with orbital periods above the period gap have an average γ velocity $\overline{\gamma} = 4.6 \pm 33.1$ km s^{-1}. They admit that part of the dispersion is due to measurement errors. For the 72 non-magnetic CVs, they determine an uncertainty in γ of 19.7 km s^{-1} calculated from the rms average of the standard deviations of the distributions of single γ measurements of the individual sources. This is too large to measure a theoretical dispersion of 15 km s^{-1} with any confidence. Assuming that this measurement error and the intrinsic dispersion add in quadrature gives their result, $\sigma_\gamma = 26.6$ km s^{-1} for longer period DN (almost twice the predicted value from Kolb & Stehle, 1996).

Figure 8 compares the distribution of γ velocities as obtained a) in this paper (solid marking) and b) from the literature (hatched lines) for the four DN observed in this pilot study. We can see that the distribution is already appearing much tighter, and the variation in the values obtained from the literature is quite large.

Initial results from the first sample of systems indicate that the behaviour of the longer-period DN does follow closely that predicted from the theory (as presented by Kolb & Stehle, 1996). The initial velocity dispersion value for the sample appears to be ~ 8 km s^{-1}. We calculated a 95 per cent confidence limit on this result, using the assumption that for a random sample (X, S^2) from a population (μ, σ^2), the quantity NS^2/σ can be described by a χ^2 distribution, with $N-1$ degrees of freedom, where N is the number of measurements in the sample. For the 95 per cent confidence interval

$$P\left(\chi^2_{0.025} < \frac{NS^2}{\sigma^2} < \chi^2_{0.975}\right) = 0.95 \qquad (5)$$

needed to be solved. Inverting the inequalities gives the 95 per cent confidence interval $4 < \sigma_\gamma < 28$ km s^{-1}. This range includes Kolb & Stehle's theoretical expectation (15 km s^{-1}), but it also agrees with van Paradijs et al.'s result. We now need to increase the sample size so as to conclusively reject or confirm the van Paradijs result. As it stands, our result provides support for the theory of Kolb & Stehle (1996).

6 CONCLUSIONS

Four long period ($P_{\rm orb} > 5$ hours) dwarf novae have been observed over a complete orbital period, in order to determine accurate absolute systemic velocities (to within ± 5 km s^{-1}). On this initial sample, the aim was to test thoroughly the methods being used to obtain the velocities, to make sure that any possible sources of error were effectively minimised. Sources of systematic error are fairly numerous using these methods, however they are very easy to identify and minimise, and in certain cases to eliminate altogether. A large sample of radial-velocity standard stars were observed, to ensure that so-called 'template mismatch' did not introduce any significant error. This enabled us to compile a list of reliable standard stars to use for future observing runs for this project. In addition, because of the high accuracy requirement for measurement of the systemic velocities, accurate measurements of other binary parameters can be made. For example, high quality radial-velocity curves mean that good semi-amplitude measurements can be obtained. Existing orbital periods can also be checked, and a value for the projected rotational velocity of the mass donor can be determined, implying that a value for the mass ratio, q, can be calculated. This value of q is then independent of the semi-amplitude value determined from the emission lines (measurements of which are uncertain and prone to error), and can then be used to determine the component masses. Doppler maps have been constructed from the Hα line profiles obtained in this study. Due to the coverage of a full orbital period, an orbit-averaged Doppler image has be created for each object. These have proved surprising. Further evidence for the existence of "sub-Keplerian" velocities is seen in the maps, as are peculiar features which may be be attributable to an outflow from the systems. These features may be peculiar to Hα emission; further investigation is needed.

Our initial results suggest that the observations agree with the theory (as set out by Kolb & Stehle, 1996). The observed velocity dispersion for the sample is ~ 8 km s^{-1}, which is smaller than the predicted value of 15 km s^{-1}. If, with further observations, this value does not alter significantly, then we can infer that the longer period systems are a

young subgroup, with an average predicted age of ≤ 1.5Gyrs. Once systemic velocities for the longer-period systems have been adequately constrained then our understanding of their kinematics and evolution will be more complete, and we can begin the search for the predicted significant difference between the velocity dispersions of CVs below and above the period gap.

Acknowledgments

The authors wish to thank the referee, Hans Ritter, for drawing our attention to the SS Cyg parallax. RCN acknowledges a studentship from the University of Southampton and a PPARC PDRA during the course of this work. The data reduction and analysis were carried out on the Southampton node of the UK STARLINK computer network. The INT is operated on the island of La Palma by the Isaac Newton Group in the Spanish Observatorio del Roque de los Muchachos of the Instituto de Astrofisica de Canarias.

REFERENCES

Barnes T. C., Moffett T. J., Slovak M. H., 1986, PASP, 98, 223
Beavers W. I., Eitter J. J., Ketelsen D. A., Oesper D. A., 1979, PASP, 91, 698
Casares J., Charles P. A., Naylor T., Pavlenko E. P., 1993, MNRAS, 265, 834
Duquennoy A., Mayor M., Halbwachs J.-L., 1991, A&AS, 88, 281
Echevarria J., Diego F., Tapia M., Costero R., Ruiz E., Salas L., Gutierrez L., Enriquez R., 1989, MNRAS, 240, 975
Eggen O. J., 1996, AJ, 111, 466
Friend M. T., Martin J. S., Connon Smith R., Jones D. H. P., 1990, MNRAS, 246, 654
Harrison T. E., McNamara B. J., Szkody P., Gilliland R. L., 2000, AJ, 120, 2649
Hellier C., 2000, NewAR, 44, 131
Hessman F. V., 1988, A&AS, 72, 515
Horne K., 1986, PASP, 98, 609
Horne K., Wade R. A., Szkody P., 1986, MNRAS, 219, 791
King A. R., 1988, QJRAS, 29, 1
Kiplinger A. L., 1979, AJ, 84, 655
Kolb U., 2001, in Vanbeveren D., ed., The influence of binaries on stellar population studies, Kluwer, Dordrecht, in press
Kolb U., Stehle R., 1996, MNRAS, 282, 1454.
Marcy G. W., Lindsay V., Wilson K., 1987, PASP, 99, 490.
Marsh, T. R., Horne, K., 1988, MNRAS, 235, 269.
North R. C., Marsh T. R., Moran C. K. J., Kolb U., Smith R. C., Stehle R., 2000, MNRAS, 313, 383
Oke J. B., Gunn J. E., 1983, ApJ, 266, 713
Patterson J., 1984, ApJS, 54, 443
Ritter H., Kolb U., 1998, A&AS, 129, 83
Schreiber M. R., Gänsicke B. T., 2001, A&A, in press
Stover R. J., Robinson E. L., Nather R. E., Montemayor T. J., 1980, ApJ, 240, 597
Thorstensen J. R., Davis M. K., Ringwald F. K., 1991, AJ, 102, 683
Tonry J., Davis M., 1979, AJ, 84, 1511
van Paradijs J., Augusteijn T., Stehle R., 1996, A&A, 312, 93
Wallace P. T., Clayton C. A., 1999, RV - Radial Components of Observer's Velocity, Starlink User Note 78
Wielen R., 1977, A&A, 60, 263
Wielen R., Dettbarn C., Fuchs B., Jahreiss H., Radons G., 1992, in Barbuy B., Renzini A., eds., The Stellar Populations of Galaxies, IAU Symp. 149, Kluwer, Dordrecht, p. 81

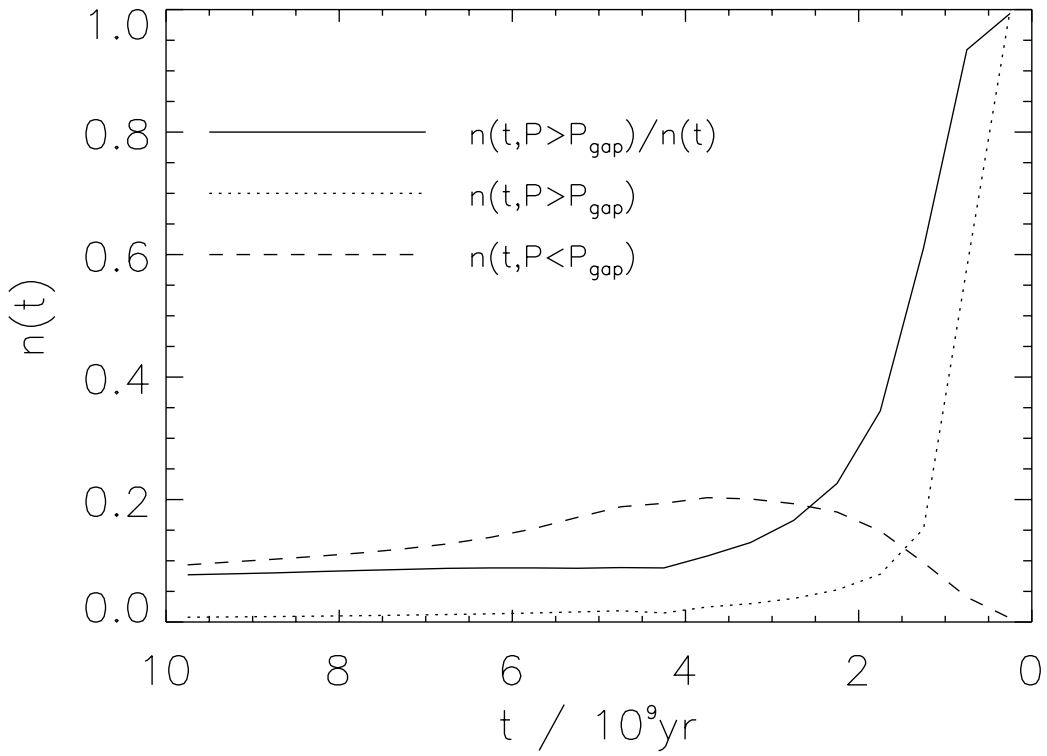
1.0
0.8
0.6
0.4
0.2
0.0
n(t)
n(t,P>P_gap)/n(t)
n(t,P>P_gap)
n(t,P<P_gap)
10
8
6
4
2
0
t / 10^9yr